J. Fluid Mech. (1997), *vol.* 352, *pp.* 359–373. Printed in the United Kingdom

Frequency downshift in three-dimensional wave trains in a deep basin

By KARSTEN TRULSEN† AND KRISTIAN B. DYSTHE

Department of Mathematics, University of Bergen, Johannes Brunsgate 12,
N–5008 Bergen, Norway

(Received 5 November 1996 and in revised form 4 August 1997)

The conservative evolution of weakly nonlinear narrow-banded gravity waves in deep water is investigated numerically with a modified nonlinear Schrödinger equation, for application to wide wave tanks. When the evolution is constrained to two dimensions, no permanent shift of the peak of the spectrum is observed. In three dimensions, allowing for oblique sideband perturbations, the peak of the spectrum is permanently downshifted. Dissipation or wave breaking may therefore not be necessary to produce a permanent downshift. The emergence of a standing wave across the tank is also predicted.

1. Introduction

The frequency downshift in the evolution of Stokes waves was first reported by Lake *et al.* (1977). They let an essentially two-dimensional uniform wave with frequency ω_0 propagate in a long tank. The uniform wave first developed sideband instabilities, dominated by the most unstable upper and lower sideband frequencies $\omega_0 \pm \delta\omega$. The wave train became strongly modulated, but then recurred as a nearly uniform wave. However, the frequency was seen to be downshifted to the most unstable lower sideband frequency $\omega_0 - \delta\omega$. Subsequently, several other experiments also showed downshift in the evolution of Stokes waves, e.g. Melville (1982), Su *et al.* (1982) and Huang, Long & Shen (1996). Downshift has also been observed in the evolution of a wave group (Su 1982), and in the evolution of bichromatic waves (Stansberg 1995). A downshift does not always happen: it has been reported to occur only when the initial steepness is sufficiently large. It has also been reported that when downshift occurs, wave breaking can be observed in the strongly modulated stage of the wave evolution.

The weakly nonlinear modulation theories for slowly modulated waves describe the evolution of wave trains that have their spectral energy narrowly distributed around a central wave vector $\boldsymbol{k}_0$, but are not limited to situations in which the central wave itself carries energy. Assuming that the steepness is $k_0 a = O(\epsilon)$ and the modulation bandwidth is $|\Delta\boldsymbol{k}|/k_0 = O(\epsilon)$, a perturbation analysis accurate to $O(\epsilon^3)$ yields the nonlinear Schrödinger (NLS) equation. In a coordinate system moving with the group velocity, the NLS equation is symmetric in the upper and lower sidebands and is thus not capable of describing a frequency shift. Taking the perturbation analysis one order higher, Dysthe (1979) derived a modified nonlinear Schrödinger (MNLS) equation which also includes the leading asymmetric effects. The broader bandwidth

† Current address: Instituto Pluridisciplinar, Universidad Complutense de Madrid, Paseo Juan XXIII 1, E–28040 Madrid, Spain.

nonlinear Schrödinger (BMNLS) equation of Trulsen & Dysthe (1996) relaxes the bandwidth constraint to $|\Delta \boldsymbol{k}|/k_0 = O(\epsilon^{1/2})$ in a theory accurate to $O(\epsilon^{7/2})$. From the stability analysis of the Stokes wave, we know that the modulation wave vector $\delta \boldsymbol{k}$ of the most unstable sidebands is such that $|\delta \boldsymbol{k}|/k_0 = O(\epsilon)$. It thus appears that the BMNLS equation should be well-suited to account for a downshift to the most unstable lower sideband, provided non-conservative effects can be properly accounted for. These equations are all special limits of the Zakharov integral equation.

The two-dimensional conservative evolution of Stokes waves has been investigated numerically with the NLS equation (e.g. Yuen & Ferguson 1978*b*), the MNLS equation (Lo & Mei 1985), the Zakharov integral equation (Caponi, Saffman & Yuen 1982) and the exact hydrodynamic equations (Dold & Peregrine 1986). If the Stokes wave has small steepness and is perturbed on a small number of unstable sidebands, the evolution is characterized by cyclic modulation and demodulation (recurrence). If the steepness is large or many unstable sidebands are perturbed, the behaviour is more complicated. By employing the more accurate theories (not NLS), the upper and lower sidebands are found to grow asymmetrically. Hence the most unstable lower sideband may become dominant temporarily. However, no permanent frequency shift has been found in the two-dimensional conservative evolution of Stokes waves.

It is commonly believed that the permanent downshift is caused by a combination of wave breaking, dissipation and nonlinear wave modulation. Proceeding along these lines, Trulsen & Dysthe (1990) added a simplified damping term to the MNLS equation to account for wave breaking, and found a permanent downshift. Hara & Mei (1991) found downshift by employing the MNLS equation modified to account for forcing by weak wind and damping by eddy viscosity. Later, Hara & Mei (1994) derived a modified MNLS equation for gravity–capillary waves forced by wind and damped by eddy viscosity, and found downshift provided the wavelength was not too short. Poitevin & Kharif (1991, 1992) and Skandrani, Kharif, & Poitevin (1996) solved the exact viscous hydrodynamic equations also accounting for surface tension and found a downshift. Uchiyama & Kawahara (1994) employed an equation originating from nonlinear optics, slightly different from the MNLS equation for water waves. They included a simplified term accounting for damping of the mean flow, and found a downshift. Kato & Oikawa (1995) endowed the MNLS equation with a damping term accounting for dissipation of the mean flow, and also found a downshift. Okamura (1996) further found downshift in the evolution of standing gravity waves. A different way of explaining the downshift is suggested in Tulin (1996), considering the conservation of energy, momentum and angular momentum in breaking waves. Based on these works, the downshift of two-dimensional Stokes waves appears to be related to damping effects in a rather insensitive manner. A rigorous account of the influence of wave breaking is however a monumental task, and is still lacking.

Three-dimensional evolution of weakly nonlinear waves has not been extensively studied. Using the NLS equation, Yuen & Ferguson (1978*a*) found that certain initial conditions can lead to perfect recurrence, while Martin & Yuen (1980) found that other initial conditions can lead to energy leakage, rendering the NLS equation potentially useless for three-dimensional computations of Stokes waves. Lo & Mei (1987) employed the MNLS equation to investigate the instability of a uniform wave train to oblique sideband perturbations. They found that the higher-order equation suppressed the energy leakage, but did not find frequency downshift.

In this paper we wish to investigate more closely the effect of oblique sideband modulation on the evolution of Stokes waves. Several experiments have been conducted in wave tanks sufficiently wide that the effect of three-dimensionality should

be considered. Our discussion is limited to narrow-banded modulation of weakly nonlinear waves (type I instability). We do not consider short-crested three-dimensional modulation for strongly nonlinear waves (type II instability), observed for instance by Su *et al.* (1982).

In a wave tank of width b, the smallest transverse wave vector component is $k_\perp = \pi/b$. For a deep-water gravity wave with central frequency f_0, the central wavenumber is $k_0 = (2\pi f_0)^2/g$, where $g \approx 9.8$ m s^{-2} is the acceleration due to gravity. The normalized transverse wave vector component will then be quantized in steps of $\Delta\mu = k_\perp/k_0$. In figure 5 of Lake *et al.* (1977), a Stokes wave with frequency 3.6 Hz propagated in a tank of width 0.91 m giving $\Delta\mu \approx 0.066$. In one of the experiments described in Huang *et al.* (1996), a Stokes wave with frequency of 2.5 Hz propagated in a tank of width 0.915 m giving $\Delta\mu \approx 0.136$. Similarly, in test 61 of Stansberg (1995), a bichromatic wave train with central frequency 1.0 Hz propagated in a tank of width 10 m giving $\Delta\mu \approx 0.078$. In all these cases, narrow-banded three-dimensional modulation is possible.

We employ the BMNLS equation of Trulsen & Dysthe (1996) because it has good bandwidth resolution to describe three-dimensional modulation. In §2 we review the BMNLS equation for application to numerical integration. The numerical method is briefly reviewed in §3. There are several ways to quantify a frequency shift, some of which are discussed in §4 aided by conservation laws for the BMNLS equation derived in the Appendix. Traditionally, and in this paper, the downshift is considered as a shift of the peak of the spectrum.

The evolution of a Stokes wave in two and three dimensions is presented in §5. The major result is that two- and three-dimensional evolution are qualitatively different. In two dimensions, without any dissipative effects added, there is no permanent shift of the peak frequency, while in three dimensions the peak frequency is permanently downshifted. In conclusion, dissipation and breaking may contribute to the experimentally observed frequency downshift, but need not be necessary unless the tank is narrow compared to the central wavelength. In addition, we predict the emergence of standing waves across the tank at large fetch.

2. The broader bandwidth modified nonlinear Schrödinger (BMNLS) equation

Trulsen & Dysthe (1996) derived the BMNLS equation correct to order $O(\epsilon^{7/2})$ for the evolution of gravity waves with steepness $k_0 a = O(\epsilon)$, bandwidth $|\Delta\boldsymbol{k}|/k_0 = O(\epsilon^{1/2})$ on water with depth $(k_0 h)^{-1} = O(\epsilon^{1/2})$. Here k_0, $\Delta\boldsymbol{k}$, a and h denote a characteristic wavenumber, modulation wave vector, amplitude and depth, respectively, while $\epsilon \ll 1$ is a small ordering parameter. The physical wave vector is $\boldsymbol{k}_0 + \Delta\boldsymbol{k}$. We will apply this equation in a long wave tank of width b, where the x-axis is along the tank, y is across and z is vertical. After all variables have been made non-dimensional by using the characteristic wavenumber k_0 and frequency $\omega_0 = (gk_0)^{1/2}$, the harmonic expansions for the velocity potential ϕ and surface displacement ζ are

$$\phi = \bar{\phi} + \tfrac{1}{2}\left(A\mathrm{e}^{\mathrm{i}\theta+z} + A_2\mathrm{e}^{2(\mathrm{i}\theta+z)} + \cdots + \text{c.c.}\right), \tag{2.1}$$

$$\zeta = \bar{\zeta} + \tfrac{1}{2}\left(B\mathrm{e}^{\mathrm{i}\theta} + B_2\mathrm{e}^{2\mathrm{i}\theta} + \cdots + \text{c.c.}\right), \tag{2.2}$$

where c.c. denotes the complex conjugate, and where $\theta = x - t$. The evolution equations for the first harmonic of the velocity potential A and the potential of the

induced slow drift $\bar{\phi}$ are

$$\frac{\partial A}{\partial t}+\frac{1}{2}\frac{\partial A}{\partial x}+\frac{\mathrm{i}}{8}\frac{\partial^2 A}{\partial x^2}-\frac{\mathrm{i}}{4}\frac{\partial^2 A}{\partial y^2}+\frac{\mathrm{i}}{2}|A|^2A$$
$$-\frac{1}{16}\frac{\partial^3 A}{\partial x^3}+\frac{3}{8}\frac{\partial^3 A}{\partial x\partial y^2}+\frac{3}{2}|A|^2\frac{\partial A}{\partial x}-\frac{1}{4}A^2\frac{\partial A^*}{\partial x}+\mathrm{i}A\frac{\partial\bar{\phi}}{\partial x}$$
$$-\frac{5\mathrm{i}}{128}\frac{\partial^4 A}{\partial x^4}+\frac{15\mathrm{i}}{32}\frac{\partial^4 A}{\partial x^2\partial y^2}-\frac{3\mathrm{i}}{32}\frac{\partial^4 A}{\partial y^4}+\frac{7}{256}\frac{\partial^5 A}{\partial x^5}-\frac{35}{64}\frac{\partial^5 A}{\partial x^3\partial y^2}+\frac{21}{64}\frac{\partial^5 A}{\partial x\partial y^4}=0 \quad \text{at} \quad z=0, \tag{2.3}$$

$$\frac{\partial\bar{\phi}}{\partial z}=\frac{1}{2}\frac{\partial|A|^2}{\partial x} \quad \text{at} \quad z=0, \tag{2.4}$$

$$\frac{\partial^2\bar{\phi}}{\partial x^2}+\frac{\partial^2\bar{\phi}}{\partial y^2}+\frac{\partial^2\bar{\phi}}{\partial z^2}=0 \quad \text{for} \quad -h<z<0, \tag{2.5}$$

$$\frac{\partial\bar{\phi}}{\partial z}=0 \quad \text{at} \quad z=-h, \tag{2.6}$$

$$\frac{\partial\bar{\phi}}{\partial y}=\frac{\partial A}{\partial y}=0 \quad \text{at} \quad y=0 \quad \text{and} \quad y=b. \tag{2.7}$$

The first harmonic of the surface displacement is given by

$$B=\mathrm{i}A+\frac{1}{2}\frac{\partial A}{\partial x}+\frac{\mathrm{i}}{8}\frac{\partial^2 A}{\partial x^2}-\frac{\mathrm{i}}{4}\frac{\partial^2 A}{\partial y^2}+\frac{\mathrm{i}}{8}|A|^2A$$
$$-\frac{1}{16}\frac{\partial^3 A}{\partial x^3}+\frac{3}{8}\frac{\partial^3 A}{\partial x\partial y^2}-\frac{5\mathrm{i}}{128}\frac{\partial^4 A}{\partial x^4}+\frac{15\mathrm{i}}{32}\frac{\partial^4 A}{\partial x^2\partial y^2}-\frac{3\mathrm{i}}{32}\frac{\partial^4 A}{\partial y^4}. \tag{2.8}$$

For application to experiments, we need to look at the slow evolution of the wave spectrum with increasing distance from the wave maker. It is convenient to introduce the moving coordinates (Lo & Mei 1985)

$$x=\eta, \qquad x/c_g-t=\xi, \tag{2.9}$$

where $c_g=1/2$ is the linear group velocity. Hence η is the distance over which the group has advanced (the fetch), while ξ is a negative time coordinate of a fixed observer. In terms of the new coordinates, the evolution equations for A and $\bar{\phi}$ become

$$\frac{\partial A}{\partial\eta}+\mathrm{i}\frac{\partial^2 A}{\partial\xi^2}-\frac{\mathrm{i}}{2}\frac{\partial^2 A}{\partial y^2}+\mathrm{i}|A|^2A+\frac{\partial^3 A}{\partial\xi\partial y^2}+8|A|^2\frac{\partial A}{\partial\xi}+4\mathrm{i}A\frac{\partial\bar{\phi}}{\partial\xi}$$
$$+\frac{3\mathrm{i}}{2}\frac{\partial^4 A}{\partial\xi^2\partial y^2}+\frac{\mathrm{i}}{8}\frac{\partial^4 A}{\partial y^4}-2\frac{\partial^5 A}{\partial\xi^3\partial y^2}-\frac{3}{4}\frac{\partial^5 A}{\partial\xi\partial y^4}=0 \quad \text{at} \quad z=0, \tag{2.10}$$

$$\frac{\partial\bar{\phi}}{\partial z}=\frac{\partial|A|^2}{\partial\xi} \quad \text{at} \quad z=0, \tag{2.11}$$

$$4\frac{\partial^2\bar{\phi}}{\partial\xi^2}+\frac{\partial^2\bar{\phi}}{\partial y^2}+\frac{\partial^2\bar{\phi}}{\partial z^2}=0 \qquad \text{for} \quad -h<z<0, \tag{2.12}$$

$$\frac{\partial\bar{\phi}}{\partial z}=0 \quad \text{at} \quad z=-h, \tag{2.13}$$

$$\frac{\partial \bar{\phi}}{\partial y} = \frac{\partial A}{\partial y} = 0 \quad \text{at} \quad y = 0 \quad \text{and} \quad y = b, \tag{2.14}$$

$$B = \mathrm{i}A + \frac{\partial A}{\partial \xi} - \frac{3\mathrm{i}}{8}|A|^2 A. \tag{2.15}$$

Incidentally, in the limit of one horizontal dimension equations (2.10)–(2.15) are equivalent to the corresponding MNLS equations.

Of primary interest for comparison with experimental observations is the first harmonic of the surface displacement. While it has been customary to solve the differential equations for A and then compute B for presentation, we find it more convenient to solve for B directly. The equations for B are identical to those for A with one additional nonlinear term:

$$\frac{\partial B}{\partial \eta} + \mathrm{i}\frac{\partial^2 B}{\partial \xi^2} - \frac{\mathrm{i}}{2}\frac{\partial^2 B}{\partial y^2} + \mathrm{i}|B|^2 B + \frac{\partial^3 B}{\partial \xi \partial y^2} + 8|B|^2 \frac{\partial B}{\partial \xi} + 2B^2 \frac{\partial B^*}{\partial \xi} + 4\mathrm{i}B\frac{\partial \bar{\phi}}{\partial \xi}$$
$$+ \frac{3\mathrm{i}}{2}\frac{\partial^4 B}{\partial \xi^2 \partial y^2} + \frac{\mathrm{i}}{8}\frac{\partial^4 B}{\partial y^4} - 2\frac{\partial^5 B}{\partial \xi^3 \partial y^2} - \frac{3}{4}\frac{\partial^5 B}{\partial \xi \partial y^4} = 0 \quad \text{at} \quad z = 0, \tag{2.16}$$

$$\frac{\partial \bar{\phi}}{\partial z} = \frac{\partial |B|^2}{\partial \xi} \quad \text{at} \quad z = 0, \tag{2.17}$$

$$4\frac{\partial^2 \bar{\phi}}{\partial \xi^2} + \frac{\partial^2 \bar{\phi}}{\partial y^2} + \frac{\partial^2 \bar{\phi}}{\partial z^2} = 0 \qquad \text{for} \quad -h < z < 0, \tag{2.18}$$

$$\frac{\partial \bar{\phi}}{\partial z} = 0 \quad \text{at} \quad z = -h, \tag{2.19}$$

$$\frac{\partial \bar{\phi}}{\partial y} = \frac{\partial B}{\partial y} = 0 \quad \text{at} \quad y = 0 \quad \text{and} \quad y = b. \tag{2.20}$$

For a numerical solution in three dimensions, the equations for B are preferred to the equations for A because they have better confinement of the instability region for the Stokes wave and are thus less susceptible to numerical instability and energy leakage. To see this, consider a Stokes wave solution, which implies

$$A = A_0 \mathrm{e}^{-\mathrm{i}A_0^2 \eta}, \qquad B = \mathrm{i}B_0 \mathrm{e}^{-\mathrm{i}B_0^2 \eta} \qquad \text{and} \qquad \bar{\phi} = 0, \tag{2.21}$$

where A_0 and B_0 are real (see (2.15)). We seek the behaviour of small perturbations in amplitude and phase

$$\begin{pmatrix} A \\ B \end{pmatrix} = (1 + a' + \mathrm{i}\theta') \begin{pmatrix} A_0 \mathrm{e}^{-\mathrm{i}A_0^2 \eta} \\ B_0 \mathrm{e}^{-\mathrm{i}B_0^2 \eta} \end{pmatrix}, \tag{2.22}$$

having the plane wave solution

$$\begin{pmatrix} a' \\ \theta' \\ \bar{\phi} \end{pmatrix} = \begin{pmatrix} \hat{a} \\ \hat{\theta} \\ \hat{\phi} \end{pmatrix} \cos(\mu y) \mathrm{e}^{\mathrm{i}(\lambda \xi - \Omega \eta)} + \text{c.c.} \tag{2.23}$$

Here μ must be an integer multiple of π/b to satisfy the boundary conditions on the sidewalls. The growth rates are given by

$$\operatorname{Im} \Omega_A = \operatorname{Im} \left(Q \left(Q - 2A_0^2 + 8A_0^2 \frac{\lambda^2}{K} \coth(Kh) \right) \right)^{1/2} \tag{2.24}$$

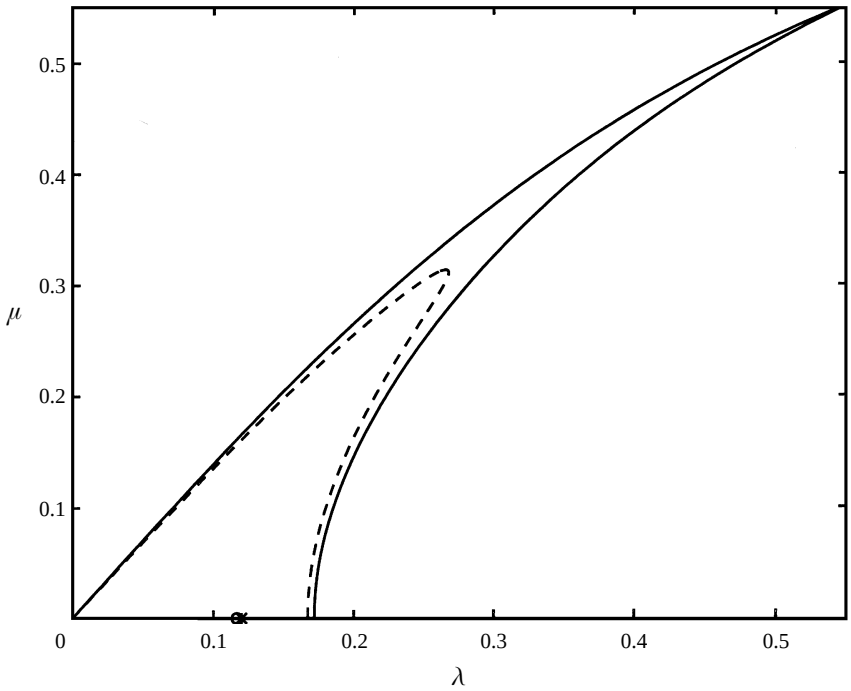

FIGURE 1. Primary instability region of a Stokes wave with $A_0 = B_0 = 0.15$ on infinite depth: —, evolution equation for A; - - -, evolution equation for B. Most unstable sideband: *, equation for A; ∘, equation for B.

and

$$\operatorname{Im}\Omega_B = \operatorname{Im}\left(Q\left(Q - 2B_0^2 + 8B_0^2\frac{\lambda^2}{K}\coth(Kh)\right) + 4B_0^4\lambda^2\right)^{1/2}, \tag{2.25}$$

where

$$Q = \lambda^2 - \tfrac{1}{2}\mu^2 - \tfrac{3}{2}\lambda^2\mu^2 + \tfrac{1}{8}\mu^4 \qquad \text{and} \qquad K = \left(4\lambda^2 + \mu^2\right)^{1/2}. \tag{2.26}$$

The additional term in (2.25) is due to the nonlinear term $B^2\partial B^*/\partial\xi$ in (2.16); its effect can be seen in figure 1. The difference in growth rate is not asymptotically significant within the order of truncation of the perturbation analysis, but it makes the system (2.16)–(2.20) preferable for numerical integration. The nonlinear term $B^2\partial B^*/\partial\xi$ is within the MNLS level of approximation, hence the equations for B have better confinement of the instability region for the MNLS equation also.

3. Numerical method

We employ the numerical method developed by Lo & Mei (1985, 1987). The two-dimensional domain (ξ, y) is discretized by a Fourier collocation method. Integration over the fetch η is done by a split-step scheme, in which the linear part of the governing equation (containing high-order derivatives) is integrated exactly in the Fourier domain, while the nonlinear part is integrated with a second-order explicit scheme in the physical domain. The linear (L) and nonlinear (N) integrations are alternated as NLLN, giving a second-order-accurate integration of the full equation.

An $M \times N$ grid of collocation points is employed for ξ and y

$$(\xi_m, y_n) = \left(\frac{2\pi m}{M\Delta\lambda}, \frac{2\pi n}{N\Delta\mu}\right) \qquad \text{for} \quad 0 \leqslant m < M \quad \text{and} \quad 0 \leqslant n < N, \tag{3.1}$$

with corresponding spectral components

$$(\lambda_i, \mu_j) = (i\Delta\lambda, j\Delta\mu) \qquad \text{for} \quad -\tfrac{1}{2}M < i \leqslant \tfrac{1}{2}M \quad \text{and} \quad -\tfrac{1}{2}N < j \leqslant \tfrac{1}{2}N. \tag{3.2}$$

The discrete Fourier transform pair is given by

$$\hat{B}(\lambda_i, \mu_j, \eta) = \frac{1}{MN} \sum_{m=0}^{M-1} \sum_{n=0}^{N-1} B(\xi_m, y_n, \eta) \mathrm{e}^{-\mathrm{i}(\lambda_i \xi_m + \mu_j y_n)} \tag{3.3}$$

and

$$B(\xi_m, y_n, \eta) = \sum_{-\frac{M}{2} < i \leqslant \frac{M}{2}} \sum_{-\frac{N}{2} < j \leqslant \frac{N}{2}} \hat{B}(\lambda_i, \mu_j, \eta) \mathrm{e}^{\mathrm{i}(\lambda_i \xi_m + \mu_j y_n)}. \tag{3.4}$$

Since ξ is a negative time coordinate of a fixed observer, λ is a frequency. The Fourier decomposition in time implies that the solution is periodic with period $2\pi/\Delta\lambda$. In practice, this requires the wave generator to be periodic as well.

The quantization in the transverse direction $\Delta\mu = \pi/b$ is imposed by the finite width b of the wave tank. The boundary conditions on the sidewalls are satisfied by requiring that the coefficients are symmetric:

$$\hat{B}(\lambda_i, \mu_j, \eta) = \hat{B}(\lambda_i, \mu_{-j}, \eta) \tag{3.5}$$

for all j.

The quantity

$$I(\eta) = \sum_{i,j} |\hat{B}(\lambda_i, \mu_j, \eta)|^2 \tag{3.6}$$

will henceforth be referred to as 'energy'. In the Appendix we show that the corresponding quantity for the continuous system is conserved. We have monitored the conservation of I to verify the accuracy of the numerical computations.

Nonlinear products are evaluated without aliasing; energy leakage should hence appear as a decrease of I. Numerical instability will on the other hand result in growth of I. We have found that numerical instability is absent provided the asymptotic bandwidth constraint is observed for the discretization of the Fourier domain; one should at least ensure that $N\Delta\lambda/2 < 1$ and $M\Delta\mu/2 < 1$.

4. Quantification of the downshift

The downshift has traditionally been considered as a shift of the peak of the spectrum. Hence one looks for the spectral component $(\lambda_{\text{peak}}, \mu_{\text{peak}})$ for which the spectrum $|\hat{B}(\lambda_i, \mu_j, \eta)|^2$ achieves its maximum. Recall that λ is the frequency corresponding to the time coordinate ξ, while η denotes the position along the wave tank.

Even though there may be transverse modulation of the wave field, experiments usually do not resolve the modulation across the wave tank. It may then be sensible to introduce the laterally integrated frequency spectrum, which has been summed across the wave tank:

$$S(\lambda_i, \eta) = \sum_j |\hat{B}(\lambda_i, \mu_j, \eta)|^2. \tag{4.1}$$

We then define $\bar{\lambda}_{\text{peak}}$ as the frequency for which $S(\lambda_i, \eta)$ achieves its maximum. For the spectrum measured by a wave gauge positioned at the midpoint between the tank walls, only the even modes (j even) would contribute to the sum (4.1).

Alternatively, one might use the mean frequency of the spectrum, defined by

$$\bar{\lambda} = \frac{\sum_{i,j} \lambda_i |\hat{B}(\lambda_i, \mu_j, \eta)|^2}{I}. \tag{4.2}$$

The one-dimensional version of this was used by Uchiyama & Kawahara (1994) and Kato & Oikawa (1995). Care should be taken when interpreting the results, as they used the spectrum of the velocity potential $|\hat{A}|^2$, while we use the spectrum of the surface displacement $|\hat{B}|^2$. In the Appendix it is shown that the means of these two spectra are not identical. While the mean of $|\hat{A}|^2$ is constant, the mean of $|\hat{B}|^2$ is not. This is indeed confirmed by our numerical computations. We believe that for application to observations, the spectrum of the surface displacement is more relevant.

There are thus at least three different choices of diagnostic frequencies (λ_{peak}, $\bar{\lambda}_{\text{peak}}$, $\bar{\lambda}$) that may be used to define a frequency shift. We monitor the evolution of these three through the numerical computations. Traditionally, and in this paper, the frequency downshift is understood as a downshift of the spectral peak, not the spectral mean.

5. Evolution of Stokes waves

We here show computations on the evolution of a Stokes wave with initial steepness $\epsilon = 0.12$ on infinite depth. In the following computations, the initial Stokes wave is perturbed on all sidebands inside a disk

$$\hat{B}(\lambda_i, \mu_j, 0) = \begin{cases} \epsilon, & \lambda_i = \mu_j = 0, \\ c, & 0 < \left(\lambda_i^2 + \mu_j^2\right)^{1/2} \leqslant 0.15, \\ 0 & \text{otherwise.} \end{cases} \tag{5.1}$$

Here c is a positive number such that the total energy is

$$I = 1.01\,\epsilon^2. \tag{5.2}$$

For the given steepness and depth, the most unstable perturbations have $\lambda = \pm 0.0986$ and $\mu = 0$, and are hence inside the perturbation region.

First we consider two- and three-dimensional evolution for the frequency discretization $\Delta\lambda = 0.1$ in a grid with $M = 16$. With this choice of parameters, the most unstable discrete modes are the first two sidebands $\lambda_{\pm 1}$. The largest modulation frequency represented is $\lambda_8 = 0.8$. For three-dimensional evolution we use the transverse discretization $\Delta\mu = 0.1$ with $N = 16$. This corresponds to a channel that is narrower than in the experiments of Lake *et al.* (1977) and Stansberg (1995) discussed in the introduction. The first quadrant of the computational grid in the Fourier domain is shown in figure 2, where the instability region for the initial Stokes wave is also indicated.

The evolution in two dimensions ($\mu = 0$) is presented in figure 3. The initial Stokes wave is perturbed on its most unstable upper and lower sidebands. In figure 3(a) the energy of these sidebands and the central wave can be studied. In figure 3(b) the frequency of the most energetic Fourier mode λ_{peak} and mean frequency $\bar{\lambda}$ are shown. The behaviour is periodic, with perfect recurrence of the Stokes wave. In each recurrence period, the frequency of the peak of the spectrum is temporarily

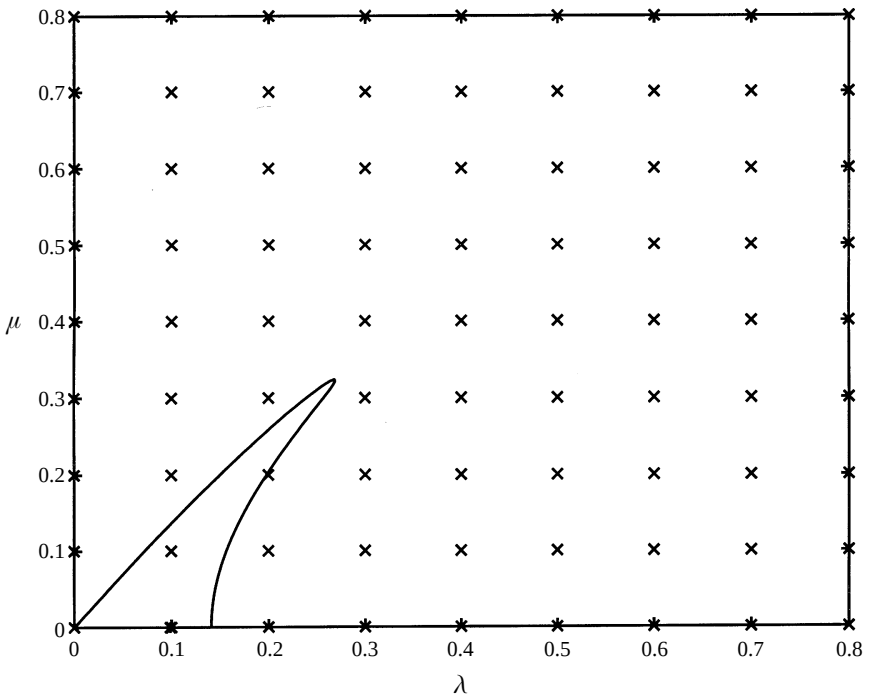

FIGURE 2. First quadrant of the modulation wave vector plane: ×, computational grid of 16×16 Fourier modes with $\Delta\lambda = \Delta\mu = 0.1$; —, instability region for a Stokes wave with steepness $\epsilon = 0.12$ on infinite depth.

downshifted, while the mean frequency is temporarily upshifted. Snapshots of the spectrum $|\hat{B}(\lambda_i, \eta)|^2$ are shown in figure 4 for three values of the fetch $\epsilon^2\eta$: for the initial perturbed Stokes wave (*a*), just before the the heavily modulated stage (*b*), and during the heavily modulated stage (*c*). Figure 4(*c*) shows how the the peak and the average frequencies are temporarily shifted in opposite directions, with a single dominating lower sideband competing with a broad tail of upper sidebands.

In figure 5 the evolution is extended to three dimensions, with uniform perturbation on the eight sidebands closest to the initial Stokes wave. The simple recurrence behaviour is suppressed. Instead, after approximately one recurrence period for the corresponding two-dimensional case, λ_{peak} and $\bar{\lambda}_{\text{peak}}$ are both downshifted to the most unstable lower sideband. The mean frequency $\bar{\lambda}$ is slightly upshifted. This new state remains unchanged for a long distance. Snapshots of the spectrum $|\hat{B}(\lambda_i, \mu_j, \eta)|^2$ are shown in figure 6 for the initial state of a near perfect Stokes wave (*a*), before the downshift (*b,c*), after the downshift (*d*), and after a long fetch (*e,f*).

Lo & Mei (1987) carried out similar computations for the three-dimensional evolution of a Stokes wave, but did not find any frequency shift. That is likely to be due to their choice of initial spectrum with perturbation energy in only four unstable sidebands with separation $\Delta\lambda = \Delta\mu = \sqrt{2}\epsilon = 0.212$ for an initial steepness $\epsilon = 0.15$. The narrow-banded modulations considered here are then effectively suppressed.

We then turn to computations with discretization $\Delta\lambda = 0.00625$ in a grid with $M = 256$. The most unstable perturbations are now represented by the two sidebands $\lambda_{\pm 16}$. The largest modulation frequency λ_{128} is still 0.8. For three-dimensional evolution we use the same transverse discretization $\Delta\mu = 0.1$ with $N = 16$, corresponding to a channel of the same width.

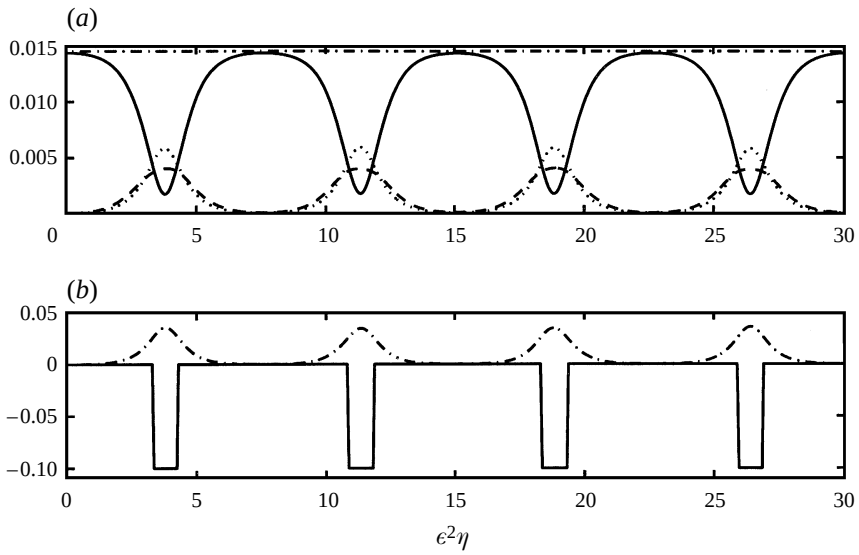

FIGURE 3. Two-dimensional evolution of a Stokes wave perturbed on its most unstable upper and lower sidebands. (*a*) Energy evolution: —, central wave $|\hat{B}(\lambda_0,\eta)|^2$; ···, first lower sideband $|\hat{B}(\lambda_{-1},\eta)|^2$; – –, first upper sideband $|\hat{B}(\lambda_1,\eta)|^2$; – · – ·, total energy I. (*b*) Frequency evolution: —, peak sideband frequency λ_{peak}; – · – ·, mean frequency $\bar{\lambda}$.

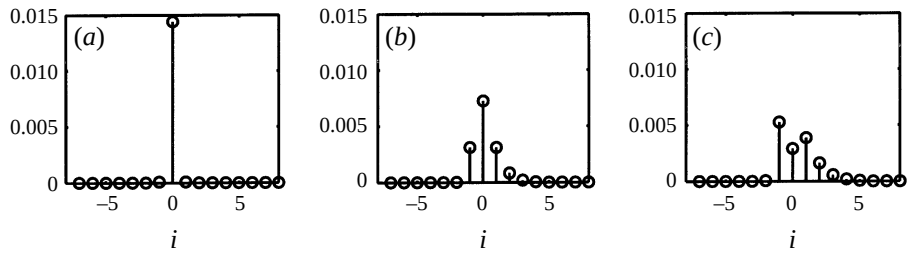

FIGURE 4. Snapshots of the spectrum $|\hat{B}(\lambda_i,\eta)|^2$ at (*a*) $\eta = 0$; (*b*) $\epsilon^2\eta = 3$; (*c*) $\epsilon^2\eta = 3.5$.

The evolution in two dimensions is presented in figure 7. The initial Stokes wave is perturbed on the nearest 46 sidebands. The two-dimensional behaviour in figure 7 no longer shows a simple recurrent behaviour because the Stokes wave has been perturbed on a large number of unstable sidebands. The energy of the initial Stokes wave is eventually smeared out over a large number of sidebands, and thus the peak of the spectrum becomes ambiguous, evidenced by the random oscillations of the peak frequency for large η. There is no permanent shift of the peak of the spectrum.

In figure 8 the evolution is extended to three dimensions, with uniform perturbation on the 116 sidebands nearest to the initial Stokes wave. The energy is sheared by a large number of sidebands. However, the peak frequencies of the spectrum λ_{peak} and $\bar{\lambda}_{\text{peak}}$ remain well-defined and are both suddenly downshifted. The mean frequency $\bar{\lambda}$ is slightly upshifted. This new state remains unchanged for a long distance. Snapshots of the spectrum $|\hat{B}(\lambda_i,\mu_j,\eta)|^2$ are shown in figure 9 for the initial state of a near perfect Stokes wave (*a*), before the downshift (*b*), during the downshift (*c*), after the downshift (*d*), and after a long fetch (*e*,*f*).

Note that in figure 9 the peak of the spectrum is not downshifted to the most unstable lower sideband, but to a sideband with transverse component $\mu_{\pm1} = \pm\Delta\mu$.

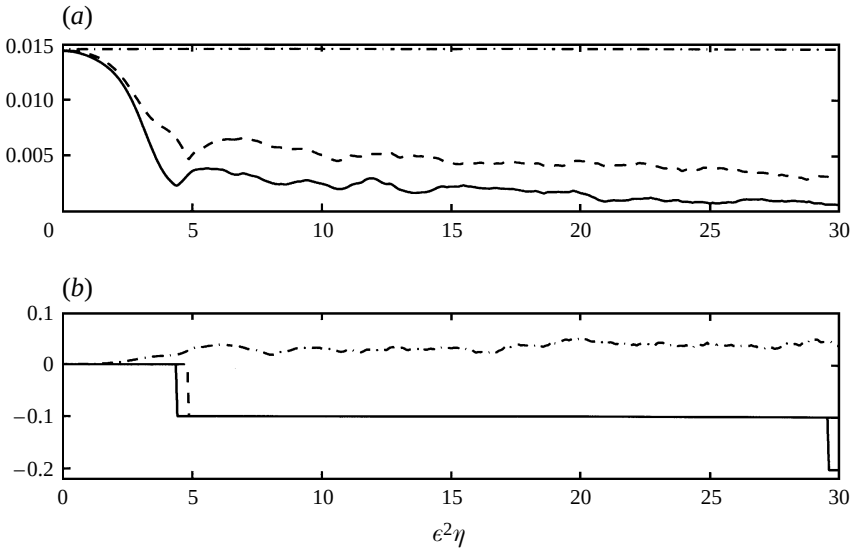

FIGURE 5. Three-dimensional evolution of a Stokes wave uniformly perturbed on the nearest eight sidebands. (*a*) Energy evolution: —, $|\hat{B}(\lambda_{\text{peak}}, \mu_{\text{peak}}, \eta)|^2$; – –, $S(\bar{\lambda}_{\text{peak}}, \eta)$, see (4.1); – · – ·, total energy I. (*b*) Frequency evolution: —, λ_{peak}; – –, $\bar{\lambda}_{\text{peak}}$; – · – ·, $\bar{\lambda}$.

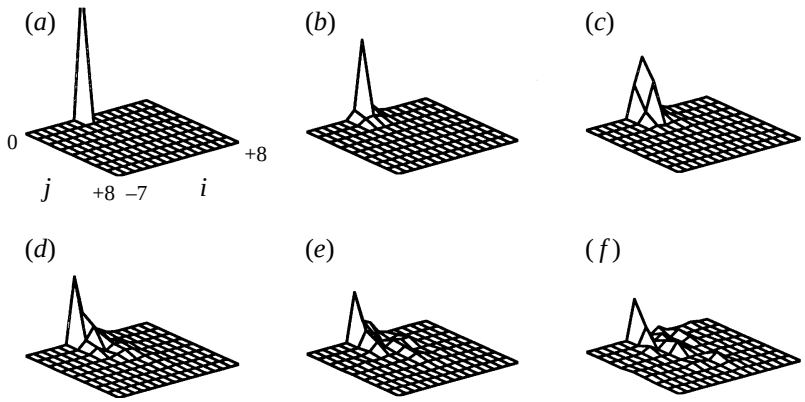

FIGURE 6. Snapshots of the spectrum $|\hat{B}(\lambda_i, \mu_j, \eta)|^2$ for $-7 \leqslant i \leqslant 8$ and $0 \leqslant j \leqslant 8$ (the spectrum is symmetric for positive and negative j): (*a*) initial state at $\eta = 0$; (*b*) $\epsilon^2\eta = 3$; (*c*) $\epsilon^2\eta = 4$ just before the downshift; (*d*) $\epsilon^2\eta = 5$ just after the downshift; (*e*) $\epsilon^2\eta = 9$; (*f*) $\epsilon^2\eta = 16$. The vertical scale has been magnified by a factor 2 in (*c–f*).

This implies the emergence of a standing wave across the wave tank with wavelength equal to twice the width of the tank.

The downshift in figure 8 happens for the non-dimensional fetch $\epsilon^2\eta \approx 7$. For application to an experiment with central frequency $f_0 = 3.6$ Hz and initial steepness $\epsilon = 0.12$, this corresponds to a dimensional fetch of approximately 9.4 m.

6. Conclusion

We have shown that computations using the conservative BMNLS equation yield qualitatively different results in two and three dimensions. In two dimensions there

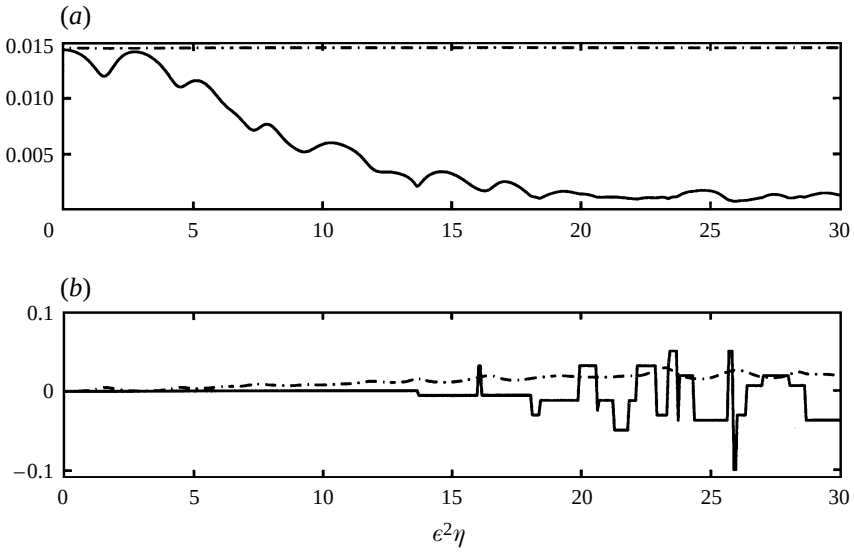

FIGURE 7. Two-dimensional evolution of a Stokes wave uniformly perturbed on the nearest 46 sidebands. (*a*) Energy evolution: —, $|\hat{B}(\lambda_{\text{peak}}, \eta)|^2$; – · – ·, total energy I. (*b*) Frequency evolution: —, λ_{peak}; – · – ·, $\bar{\lambda}$.

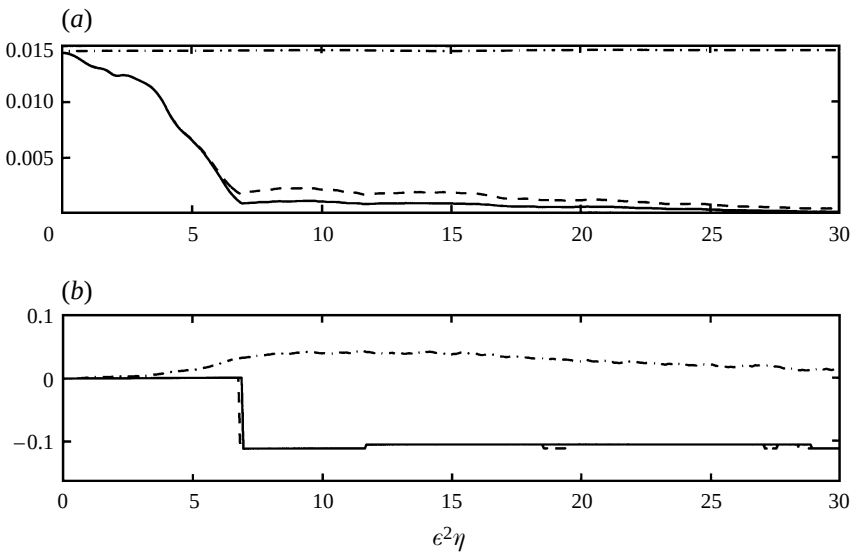

FIGURE 8. Three-dimensional evolution of a Stokes wave uniformly perturbed on the nearest 116 sidebands. (*a*) Energy evolution. (*b*) Frequency evolution. See caption of figure 5 for line styles.

is no permanent shift of the peak frequency. In three dimensions, the peak frequency can be downshifted and standing waves across the tank can arise as a consequence of slow and weakly nonlinear wave modulation. We have found that numerical computations using the MNLS equation also show the same qualitative result, while the NLS equation does not yield a frequency shift. The three-dimensional conservative downshift is therefore likely to be due to the asymmetric terms found by Dysthe (1979). However, due to the broadening of the bandwidth experienced in three-

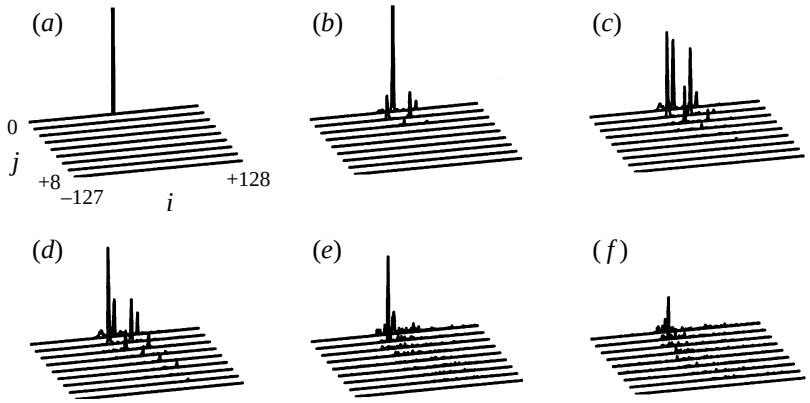

FIGURE 9. Snapshots of the spectrum $|\hat{B}(\lambda_i, \mu_j, \eta)|^2$ for $-127 \leqslant i \leqslant 128$ and $0 \leqslant j \leqslant 8$ (the spectrum is symmetric for positive and negative j): (*a*) initial state at $\eta = 0$ (the top of the peak at $i = j = 0$ has been truncated); (*b*) $\epsilon^2\eta = 6$ before the downshift; (*c*) $\epsilon^2\eta = 7$ during the downshift; (*d*) $\epsilon^2\eta = 8$ after the downshift; (*e*) $\epsilon^2\eta = 14$; (*f*) $\epsilon^2\eta = 22$. The vertical scale has been magnified by a factor 2 in (*c–f*).

dimensional evolution, we feel that the broader bandwidth equation is more satisfying for this application. The MNLS and BMNLS equations are both special limits of the Zakharov integral equation, thus we anticipate that the same result can also be obtained by the latter.

The downshift of the peak frequency reported here does not require dissipation or wave breaking. However, for sufficiently narrow laboratory wave tanks, narrow-banded transverse modulation will be suppressed, and the present explanation of the downshift cannot be used. In reality, the full explanation of the downshift probably involves the combined effects of three-dimensional nonlinear modulation, dissipation and wave breaking.

This research has been supported by the Norwegian Research Council through a fellowship (NFR 109328/410) and a grant for computing time (Programme for Supercomputing).

Appendix. Conservation laws

In §2 we reviewed three different forms of the BMNLS equation. To obtain conservation laws valid for all three forms, we consider a generalization of the BMNLS equation with arbitrary coefficients, having all of the above evolution equations as special cases. The complex amplitude a denotes the first harmonic of a wave train. Linear dissipation is included through the coefficient d_0. With real coefficients α, β, d_0 and c_i for $i = 0, 1, \ldots, 15$, we consider the system

$$\begin{aligned}\frac{\partial a}{\partial t} + (d_0 + \mathrm{i}c_0)a + c_1\frac{\partial a}{\partial x} + \mathrm{i}c_2\frac{\partial^2 a}{\partial x^2} + \mathrm{i}c_3\frac{\partial^2 a}{\partial y^2} + \mathrm{i}c_4|a|^2 a + c_5\frac{\partial^3 a}{\partial x^3} + c_6\frac{\partial^3 a}{\partial x \partial y^2} \\ + c_7|a|^2\frac{\partial a}{\partial x} + c_8 a^2\frac{\partial a^*}{\partial x} + \mathrm{i}c_9 a\frac{\partial \bar{\phi}}{\partial x} + \mathrm{i}c_{10}\frac{\partial^4 a}{\partial x^4} + \mathrm{i}c_{11}\frac{\partial^4 a}{\partial x^2 \partial y^2} + \mathrm{i}c_{12}\frac{\partial^4 a}{\partial y^4} + c_{13}\frac{\partial^5 a}{\partial x^5} \\ + c_{14}\frac{\partial^5 a}{\partial x^3 \partial y^2} + c_{15}\frac{\partial^5 a}{\partial x \partial y^4} = 0 \quad \text{at} \quad z = 0 \end{aligned} \tag{A 1}$$

$$\frac{\partial\bar{\phi}}{\partial z} = \beta\frac{\partial|a|^2}{\partial x} \quad \text{at} \quad z = 0 \tag{A 2}$$

$$\alpha^2\frac{\partial^2\bar{\phi}}{\partial x^2} + \frac{\partial^2\bar{\phi}}{\partial y^2} + \frac{\partial^2\bar{\phi}}{\partial z^2} = 0 \quad \text{for} \quad -h < z < 0 \tag{A 3}$$

$$\frac{\partial\bar{\phi}}{\partial z} = 0 \quad \text{at} \quad z = -h \tag{A 4}$$

The Fourier transform of $a(\boldsymbol{x})$ is denoted by $\hat{a}(\boldsymbol{k})$,

$$\hat{a}(\boldsymbol{k}) = \frac{1}{(2\pi)^2}\int a(\boldsymbol{x})\exp(-\mathrm{i}\boldsymbol{k}\cdot\boldsymbol{x})\,\mathrm{d}\boldsymbol{x}, \qquad a(\boldsymbol{x}) = \int \hat{a}(\boldsymbol{k})\exp(\mathrm{i}\boldsymbol{k}\cdot\boldsymbol{x})\,\mathrm{d}\boldsymbol{k}, \tag{A 5}$$

with $\boldsymbol{x} = (x, y)$ and $\boldsymbol{k} = (\lambda, \mu)$. The results in this section are derived for an infinite domain in $\boldsymbol{x}$ with sufficiently rapidly vanishing boundary conditions on $a(\boldsymbol{x})$ as $|\boldsymbol{x}| \to \infty$. These results are still valid for a finite domain $0 \leqslant y \leqslant b$ with vanishing normal derivatives on the sidewalls, or for a periodic domain in x. Then λ and μ will take discrete values λ_i and μ_j, and integration over λ and μ will become summation over λ_i and μ_j.

It is convenient to introduce the quantities

$$I_a(t) = \int |a|^2\,\mathrm{d}\boldsymbol{x} = (2\pi)^2\int |\hat{a}|^2\,\mathrm{d}\boldsymbol{k} \tag{A 6}$$

and

$$J_a(t) = \int\left(\frac{\mathrm{i}}{2}a\frac{\partial a^*}{\partial x} + \text{c.c.}\right)\mathrm{d}\boldsymbol{x} = (2\pi)^2\int \lambda|\hat{a}|^2\,\mathrm{d}\boldsymbol{k}. \tag{A 7}$$

The mean of λ in the spectrum $|\hat{a}|^2$ is then

$$\bar{\lambda}_a = \frac{J_a}{I_a}. \tag{A 8}$$

It is readily found that

$$\frac{\mathrm{d}I_a}{\mathrm{d}t} = -2d_0 I_a \tag{A 9}$$

and

$$\frac{\mathrm{d}J_a}{\mathrm{d}t} = c_8\int\left(-\mathrm{i}\left(a\frac{\partial a^*}{\partial x}\right)^2 + \text{c.c.}\right)\mathrm{d}\boldsymbol{x} - 2d_0 J_a \tag{A 10}$$

In (2.10) for the evolution of the first harmonic of the velocity potential A over fetch η, the coefficients c_8 and d_0 are zero. Hence substituting A for a, the corresponding I_A, J_A and the mean $\bar{\lambda}_A$ are all constant. Even with linear dissipation $d_0 > 0$ included, it is seen that the decay rates of I_A and J_A are equal, and hence the mean of the spectrum $\bar{\lambda}_A$ is still constant.

In (2.16) for the evolution of the first harmonic of the surface displacement B over fetch η, we have $c_8 > 0$ while $d_0 = 0$. Hence substituting B for a, the corresponding I_B is constant, but J_B is not constant due to the nonlinear term $B^2\partial B^*/\partial\xi$. From (2.15) we have to a leading approximation

$$\hat{B} \approx \mathrm{i}(1+\lambda)\hat{A}. \tag{A 11}$$

For positive c_8, the mean of the spectrum $\bar{\lambda}_B$ should therefore initially be upshifted if $|\hat{B}|^2$ is initially symmetrically distributed around $\lambda = 0$. This is confirmed by our numerical results.

REFERENCES

Caponi, E. A., Saffman, P. G. & Yuen, H. C. 1982 Instability and confined chaos in a nonlinear dispersive wave system. *Phys. Fluids* **25**, 2159–2166.

Dold, J. W. & Peregrine, D. H. 1986 Water-wave modulation. In *Proc. 20th Intl Conf. on Coastal Engineering, Taipei* (ed. B. L. Edge), vol. 1, pp. 163–175. ASCE.

Dysthe, K. B. 1979 Note on a modification to the nonlinear Schrödinger equation for application to deep water waves. *Proc. R. Soc. Lond.* A **369**, 105–114.

Hara, T. & Mei, C. C. 1991 Frequency downshift in narrowbanded surface waves under the influence of wind. *J. Fluid Mech.* **230**, 429–477.

Hara, T. & Mei, C. C. 1994 Wind effects on the nonlinear evolution of slowly varying gravity–capillary waves. *J. Fluid Mech.* **267**, 221–250.

Huang, N. E., Long, S. R. & Shen, Z. 1996 The mechanism for frequency downshift in nonlinear wave evolution. *Adv. Appl. Mech.* **32**, 59–117.

Kato, Y. & Oikawa, M. 1995 Wave number downshift in modulated wavetrain through a nonlinear damping effect. *J. Phys. Soc. Japan* **64**, 4660–4669.

Lake, B. M., Yuen, H. C., Rungaldier, H. & Ferguson, W. E. 1977 Nonlinear deep-water waves: theory and experiment. Part 2: Evolution of a continuous wave train. *J. Fluid Mech.* **83**, 49–74.

Lo, E. & Mei, C. C. 1985 A numerical study of water-wave modulation based on a higher-order nonlinear Schrödinger equation. *J. Fluid Mech.* **150**, 395–416.

Lo, E. Y. & Mei, C. C. 1987 Slow evolution of nonlinear deep water waves in two horizontal directions: A numerical study. *Wave Motion* **9**, 245–259.

Martin, D. U. & Yuen, H. C. 1980 Quasi-recurring energy leakage in the two-space-dimensional nonlinear Schrödinger equation. *Phys. Fluids* **23**, 881–883.

Melville, W. K. 1982 The instability and breaking of deep-water waves. *J. Fluid Mech.* **115**, 165–185.

Okamura, M. 1996 Long time evolution of standing gravity waves in deep water. *Wave Motion* **23**, 279–287.

Poitevin, J. & Kharif, C. 1991 Subharmonic transition of a nonlinear wave train on deep water. In *Mathematical and Numerical Aspects of Wave Propagation Phenomena* (ed. G. C. Cohen, L. Halpern & P. Joly), pp. 567–576. SIAM.

Poitevin, J. & Kharif, C. 1992 Subharmonic transition of a nonlinear short gravity wave train on deep water. In *Proc. Nonlinear Water Waves Workshop* (ed. D. H. Peregrine), pp. 54–63. University of Bristol

Skandrani, C., Kharif, C. & Poitevin, J. 1996 Nonlinear evolution of water surface waves: the frequency down-shift phenomenon. *Contemp. Maths* **200**, 157–171.

Stansberg, C. T. 1995 Spatially developing instabilities observed in experimental bichromatic wave trains. In *26th IAHR Congress (HYDRA 2000)* (ed. A. J. Grass), vol. 3, pp. 180–185. Thomas Telford.

Su, M.-Y. 1982 Evolution of groups of gravity waves with moderate to high steepness. *Phys. Fluids* **25**, 2167–2174.

Su, M.-Y., Bergin, M., Marler, P. & Myrick, R. 1982 Experiments on nonlinear instabilities and evolution of steep gravity-wave trains. *J. Fluid Mech.* **124**, 45–72.

Trulsen, K. & Dysthe, K. B. 1990 Frequency down-shift through self modulation and breaking. In *Water Wave Kinematics* (ed. A. Tørum & O. T. Gudmestad), pp. 561–572. Kluwer.

Trulsen, K. & Dysthe, K. B. 1996 A modified nonlinear Schrödinger equation for broader bandwidth gravity waves on deep water. *Wave Motion* **24**, 281–289.

Tulin, M. P. 1996 Breaking of ocean waves and downshifting. In *Waves and Nonlinear Processes in Hydrodynamics* (ed. J. Grue, B. Gjevik & J. E. Weber), pp. 177–190. Kluwer.

Uchiyama, Y. & Kawahara, T. 1994 A possible mechanism for frequency down-shift in nonlinear wave modulation. *Wave Motion* **20**, 99–110.

Yuen, H. C. & Ferguson, W. E. 1978*a* Fermi–Pasta–Ulam recurrence in the two-space dimensional nonlinear Schrödinger equation. *Phys. Fluids* **21**, 2116–2118.

Yuen, H. C. & Ferguson, W. E. 1978*b* Relationship between Benjamin–Feir instability and recurrence in the nonlinear Schrödinger equation. *Phys. Fluids* **21**, 1275–1278.